SCIENTIFIC REPORTS

Erschienen in: Scientific Reports ; 3 (2013). - 1116

OPEN

SUBJECT AREAS:
SUPER-RESOLUTION MICROSCOPY
CELLULAR IMAGING
TECHNIQUES AND INSTRUMENTATION
OPTICAL TECHNIQUES

Received
14 November 2012

Accepted
18 December 2012

Published
23 January 2013

Correspondence and requests for materials should be addressed to M.L. (leiming@opt.ac.cn) or B.Y. (yaobl@opt.ac.cn)

DMD-based LED-illumination Super-resolution and optical sectioning microscopy

Dan Dan[1], Ming Lei[1], Baoli Yao[1], Wen Wang[2], Martin Winterhalder[3], Andreas Zumbusch[3], Yujiao Qi[1], Liang Xia[2], Shaohui Yan[1], Yanlong Yang[1], Peng Gao[1], Tong Ye[1] & Wei Zhao[1]

[1]State Key Laboratory of Transient Optics and Photonics, Xi'an Institute of Optics and Precision Mechanics, Chinese Academy of Sciences, Xi'an 710119, China, [2]Department of Anatomy & K. K. Leung Brain Research Centre, Fourth Military Medical University, Xi'an 710032, China, [3]Department of Chemistry, University of Konstanz, D-78457 Konstanz, Germany.

Super-resolution three-dimensional (3D) optical microscopy has incomparable advantages over other high-resolution microscopic technologies, such as electron microscopy and atomic force microscopy, in the study of biological molecules, pathways and events in live cells and tissues. We present a novel approach of structured illumination microscopy (SIM) by using a digital micromirror device (DMD) for fringe projection and a low-coherence LED light for illumination. The lateral resolution of 90 nm and the optical sectioning depth of 120 μm were achieved. The maximum acquisition speed for 3D imaging in the optical sectioning mode was 1.6×10^7 pixels/second, which was mainly limited by the sensitivity and speed of the CCD camera. In contrast to other SIM techniques, the DMD-based LED-illumination SIM is cost-effective, ease of multi-wavelength switchable and speckle-noise-free. The 2D super-resolution and 3D optical sectioning modalities can be easily switched and applied to either fluorescent or non-fluorescent specimens.

Despite of the availability of various high resolution microscopic technologies, e.g., scanning electron microscopy (SEM), scanning tunnel microscopy (STM), atomic force microscopy (AFM), optical microscopy plays an essential role in biological studies. The key advantages, especially of far-field optical microscopy, over other forms of microscopy are the capability and compatibility of non-contact, minimally invasive observation and measurement of live specimens. However, the spatial resolution of conventional far-field optical microscopy is limited to about 200 nm, due to the well-known Abbe diffraction-limit. This is larger than many subcellular structures to be resolved. Over the past decade, this limitation has driven the exploration of super-resolution optical imaging methodologies. A number of far-field optical super-resolution microscopic techniques, such as Stimulated Emission Depletion (STED) microscopy[1–3], Structured Illumination Microscopy (SIM)[4,5], Stochastic Optical Reconstruction Microscopy (STORM)[6,7], Photo-Activated Localization Microscopy (PALM)[8] and so forth have since been developed.

As a wide-field optical microscopy, SIM has found widespread applications for investigations of subcellular structures[9–11] and for time-series imaging of living cells[12–15] due to its resolution beyond the diffraction-limit, its axial sectioning capability, as well as its high imaging speed. SIM was first introduced by Neil *et al.*[16] as a means to eliminate the out-of-focus background encountered in wide-field microscopy and to improve its signal-to-noise ratio. By projecting a spatial fringe pattern onto an object, only the zero spatial frequency does not attenuate with defocus. As a result, the microscope images efficiently only the portion of object where the fringe pattern is focused in. Simple processing of wide-field images acquired with three lateral shifted patterns permits an optically sectioned image to be extracted in real-time. The axial resolution of SIM can be as good as that of the confocal microscope. Moreover, there have been numerous attempts to exploit SIM to achieve different goals. Notably, Gustafsson *et al.*[17] used basically the same principle to improve the lateral resolution by a factor of two in its linear form, and by a larger factor in a nonlinear form[18]. The improvement of resolution is obtained by shifting additional components of the object spectrum into the microscope's optical transfer function (OTF) domain through a frequency mixing process. Like this, a Moiré pattern is generated by the patterned illumination. Although the Moiré pattern detected by the objective is a low frequency pattern, it contains the high frequency information of the sample. Accordingly, by extraction of the additional high frequency components, the high resolution image can be reconstructed.

In SIM, the optical sectioning strength and the spatial resolution will increase as the spatial frequency of the illuminating fringes increases. Commonly, sinusoidal fringe illumination with a spatial frequency near the cut-off frequency of the microscope's OTF is essential. The required fringes can be generated by laser beams interference. Originally, the phase-shifted sinusoidal fringe was produced by mechanical motion of a diffraction grating, which had a low speed and low precision of phase shifts[9,17]. The SIM frame-rate can be increased drastically by using a spatial light modulator (SLM), which has the advantage of generating and controlling the fringe patterns accurately and quickly[19]. State-of-art ferroelectric liquid crystal on silicon spatial light modulators (LCOS-SLM) allows higher reflectivity and frame-rates. They have already been used in SIM with total internal reflection mode[15,20], as well as in 3D live cell imaging[14]. However, because such devices are polarization-dependent and purely phase modulated, their applications are typically confined to a single excitation wavelength. For maximal interference contrast, the two beams need to be parallel linearly polarized, hence the implementation of polarization control with two liquid crystal switchable retarders is technically demanded. In addition, the high coherence of laser inevitably produces speckle-noise, which will seriously degrade the image quality. Dynamic averaging of the speckle-noise by using a rotating diffuser or random waggling of the homogenizers such as multimode fibers phase modulator will give a smooth image, but also limit the image acquisition speed and increase the complexity of the system.

In this paper, we propose a novel structured illumination microscope using a fringe projection scheme that combines a computer-controlled digital micromirror device (DMD) with a LED-illumination. The LED is a widely-used and cost-effective light source with relatively narrow emission bandwidths but low spatial coherence. The latter property impedes the generation of speckle-noise. The DMD is a micro-electro-mechanical system (MEMS) consisting of hundred thousands of tiny switchable mirrors with two stable mirror states (+12 degrees and −12 degrees). When a micromirror is set at +12 degrees toward the illumination, it is referred to as "on" state. Similarly, at the position at −12 degrees it is referred to as "off" state. The mirrors are highly reflective and have higher refreshing speed and broader spectral response compared with ordinary LCOS-SLMs. These features make DMDs attractive for many applications in microscopy. Liang *et al.*[21] developed a programmable array microscope (PAM) incorporating a DMD to provide programmable confocal scanning with increased efficiency and frame-rate. Zheng *et al.*[22] realized a DMD-based optical scatter imaging approach to probing localized particle size in situ. Jiang *et al.*[23] used a DMD instead of a rotating diffuser to get speckle-illuminated fluorescence confocal microscope. As a high efficiency and fast spatial light modulator, DMD has also been used in fringe projection applications. Zhang *et al.*[24] reached a 667 Hz 3D shape measurement by using DMD to switch structured patterns. Fukano *et al.*[25] developed a wide-field fluorescence microscope equipped with a DMD to acquire optically sectioned images and to detect fluorescence resonance energy transfer (FRET) between cyan and yellow mutants of green fluorescent protein[26]. With the DMD-based SIM proposed here, spatial resolution down to 90 nm is demonstrated by imaging gold nano-particles and dye-labeled BPAE cells. The optical sectioning capability of the system is shown by imaging pollen grains and Golgi-stained mouse brain neurons. An acquisition speed of 1.6×10^7 pixels/second with a resolution of 1024×768 pixels has been achieved in optical sectioning mode. This value is mainly determined by the exposure time and readout rate of the camera.

Results

DMD-based LED-illumination SIM system. The schematic diagram of the proposed DMD-based LED-illumination SIM system is shown in Fig. 1. High brightness LEDs with switchable wavelengths of 365 nm, 405 nm, 450 nm and 530 nm serve as excitation sources. LED-illumination has the advantages of being low-cost, ease of use, and free of speckle-noise. Benefiting from the reflection broad spectrum of DMD chip, multi-wavelength excitation can be implemented. Because the DMD chip is reflective and works at small incident angle, the illumination and projection lights have their paths very close to each other in front of the chip. It needs a long path to separate them well, which increases the overall path length of the system. In order to make the microscope system more compact, we employed a total internal reflection (TIR) prism[27] to separate the illumination and the projection paths in minimal space. As shown in Fig. 1, the nearly collimated LED light enters the TIR-Prism, undergoes total internal reflection within the prism, and illuminates the DMD chip. Light modulated by the DMD passes through the TIR-Prism, is collimated by an achromatic collimating lens, before being reflected by a dichroic beamsplitter into the back aperture of a 100× objective (Apo TIRF, NA1.49, Nikon Inc., Japan) or a 20× objective (EO M Plan HR, NA0.6, 13 mm working distance, Edmund Optics Inc., USA). Sliding the collimating lens will slightly change the divergence of the illumination beam. This ensures that the fringe patterns on the DMD chip is precisely projected on the focal plane. The demagnification of the projection system is 176 for the 100× objective. The sample is mounted on a manual XY and Z-axis motorized translation stage (M-405.PG, Physik Instrumente Inc., Germany) that can be moved axially in minimum step of 50 nm. A USB CCD camera (DCU223M, 1024×768 pixels with pixel size of 4.65×4.65 μm^2, Thorlabs Inc., USA) is employed to capture the 2D image with a zoom lens (70–300 mm, F/4-5.6, Nikon Inc., Japan), which incorporated with the objective lens produces a variable magnification of the image. The CCD camera has a maximum full-frame rate of 27 fps at its minimal exposure time. A long-pass filter is inserted in front of the zoom lens to block the excitation beam for fluorescence imaging. Automated data collection, DMD patterns generation, and motorized stage movement are implemented by custom software programmed in C++.

Super-resolution imaging. To evaluate the spatial resolution of the DMD-based SIM microscope, we used gold nano-particles (80 nm-diameter) deposited on 170 μm-thick coverslips as test samples. The Abbe resolution limit is ~151 nm calculated for the 100× objective of NA=1.49 at the wavelength of 450 nm. The FWHMs were measured and averaged from 50 gold nano-particles. The resultant FWHM for the SIM is 90±10 nm, which is much better than that of the conventional microscopy, i.e., 225±5 nm. Figure 2 presents the obtained images from both conventional illumination mode and the SIM with the 450 nm wavelength of LED.

Similar results were obtained with the BPAE cells slice. The intracellular mitochondrial network was stained with the fluorescent dye MitoTracker Red CMXRos. Under the excitation of 530 nm LED, the fluorescence image of the structure of mitochondria were clearly visible under the 100× objective of NA=1.49, with a long-pass filter (LP570 nm) in front of the CCD camera. The SIM image again features much improved lateral resolution over the conventional wide-field microscopy, as shown in Fig. 3.

To obtain a near isotropic resolution, multi-orientation illuminations are generally required. In our experiments, we applied two perpendicular illumination fringe orientations, i.e., X and Y directions (0° and 90°) to achieve higher imaging speed and simplify the pattern design and data analysis. Nevertheless, it is possible to generate three-orientation illumination (0°, 60°, 120°)[14] or four-orientation illumination (0°, 45°, 90°, 135°)[19] with specifically designed illumination patterns.

Optical sectioning imaging. As a benefit of the fringe projection and low-coherence LED-illumination, DMD-based SIM also has optical sectioning capability free of speckle-noise. As an example, we used

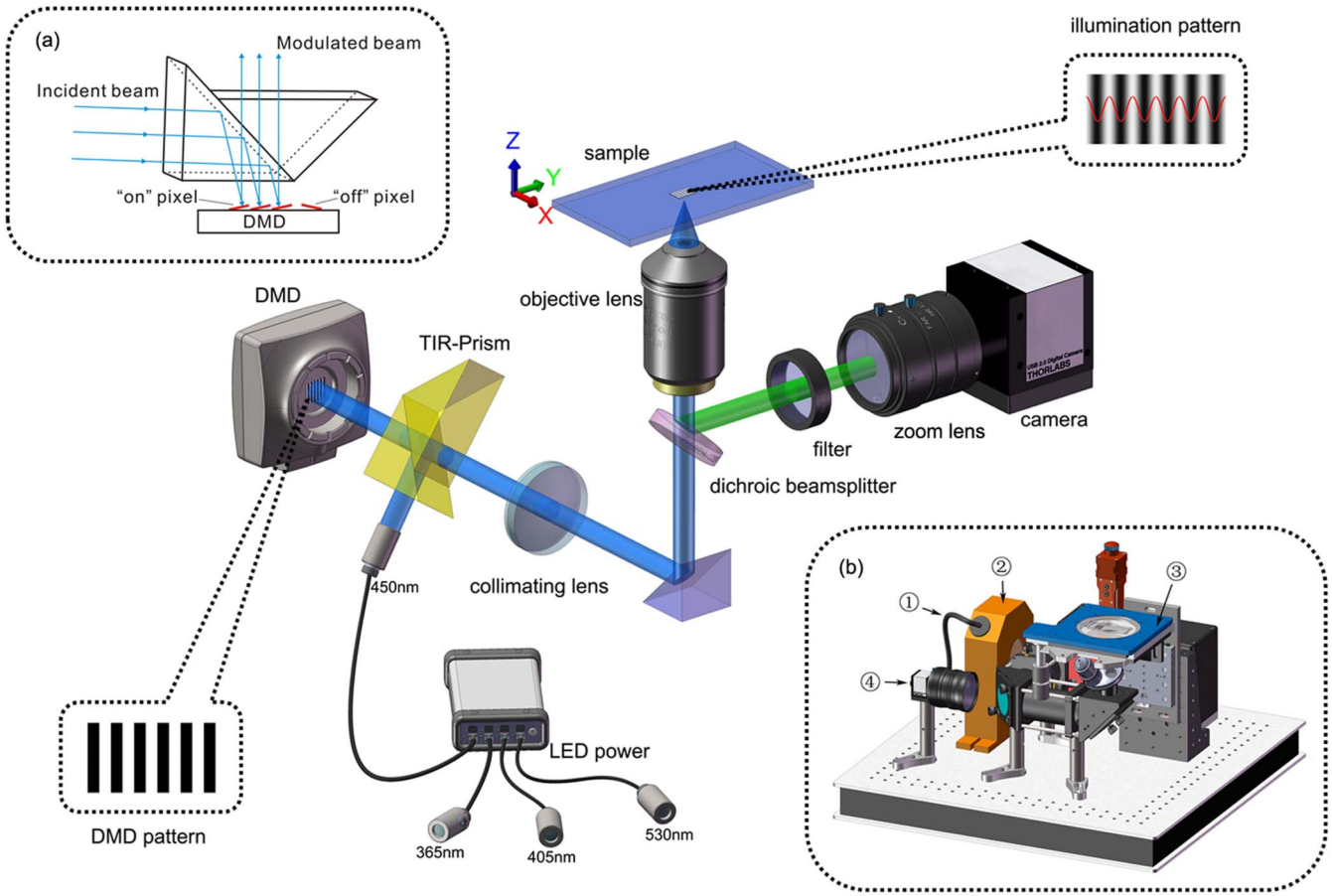

Figure 1 | Scheme of the DMD-based LED-illumination SIM microscope. A low-coherence LED light is introduced to the DMD via a TIR-Prism. The binary fringe pattern on DMD is demagnified and projected onto the specimen through a collimating lens and a microscope objective lens. Higher orders of spatial frequencies of the binary fringe are naturally blocked by the optics, leading to a sinusoidal fringe illumination in the sample plane. Fluorescence or scattered light from the specimen is directly imaged onto the CCD or CMOS camera. Inset (a) shows the principle of the TIR-Prism. The illumination light enters the prism and reflects through total internal reflection (TIR) within the prism and illuminates the DMD. Each micromirror of the DMD has an "on" position of +12° and an "off" position of −12° from the normal of the DMD. As a result, the illumination light is introduced at 24° from the normal so that the mirrors reflect the light at 0° when working at the "on" state. Inset (b) gives the configuration of the system, including the LED light guide ①, the DMD unit ②, the sample stage ③, and the CCD camera ④.

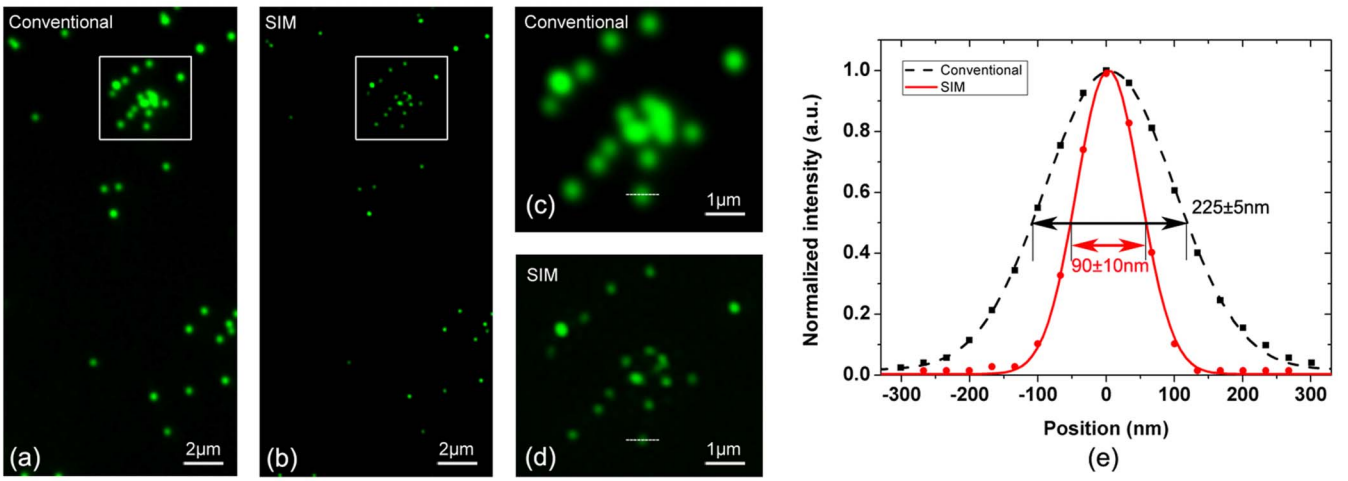

Figure 2 | Determination of the lateral SIM resolution using 80 nm-diameter gold nano-particles. As a comparison, image (a) was captured in the conventional illumination mode, and (b) is a SIM image. Zooms are shown in (c) and (d). The line-scans of a selected nano-particle in (c) and (d) are plotted in (e). The experiment was performed with the 100× objective of NA=1.49 at a LED wavelength of 450 nm.

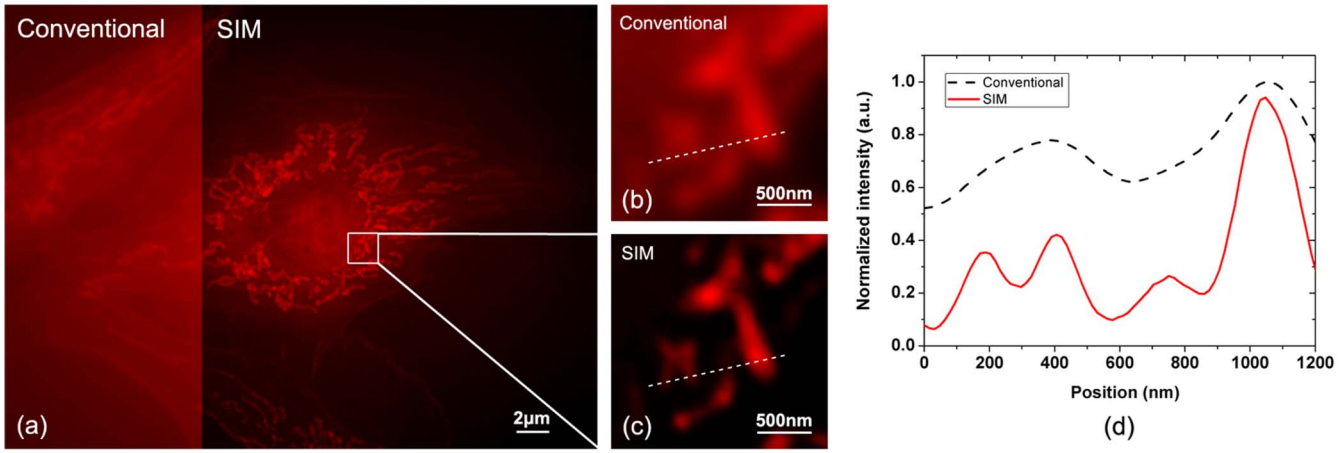

Figure 3 | Images obtained by SIM and conventional wide-field microscopy for BPAE cells stained with MitoTracker Red CMXRos. The left portion of the entire image (a) is obtained with conventional illumination, and the right portion is the result of a SIM recording. Zooms are shown in (b) and (c). The line-scans of selected parts in (b) and (c) are plotted in (d). The experiment was performed with the 100× objective of NA=1.49. The fluorescence signal from the BPAE cells was excited with a 530 nm LED, and detected by the CCD camera with a long-pass filter (LP570 nm).

the setup for imaging a pollen grain specimen which exhibits strong autofluorescence under the excitation with 450 nm LED light. Figure 4(a) shows a stack of images of the thick volume structure of the pollen grains with the 20×, NA=0.6, long working distance objective. We sliced 303 layers of the volume and captured 909 raw images in 1024×768 pixels. The axial slice interval was 400 nm, thus the slicing depth was 120.8 μm. The acquisition time of the SIM volume was 58 s, including 24 ms exposure time plus 36 ms readout time of the CCD camera for each raw image, 10 ms Z-stage settle time for each slicing layer, and 31 μs loading time for each DMD illumination fringe pattern. Figure 4(b) presents the maximum-intensity projection of the 303 planes along Z-axis. The dimension of the biggest pollen grain is about 100 μm in diameter. This figure demonstrates the capability of out-of-focus light rejection and optical sectioning of SIM. The Supplementary Movie 1 shows the "3D image" of the pollen grains observed from different angles after 3D reconstruction by using the ImageJ.

Another merit of the DMD-based LED-illumination SIM worthwhile mentioning is that it can be used for non-fluorescent specimens. For instance, we used the apparatus for obtaining the 3D structure of Golgi-stained mouse brain neurons. Figure 5(a) shows a stack of Golgi-stained neuron cells with the 20×, NA=0.6 objective under the illumination of 450 nm LED light. Here the dichroic beamsplitter in Fig. 1 was replaced by a 50 : 50 broadband beamsplitter and the filter in front of the zoom lens was removed. 186 slicing layers consisting of 558 raw images in 1024×768 pixels were captured with an axial slice interval of 400 nm. Since the contrast of the Golgi-stained specimen coming from the back-reflection and scattering of illumination light by the microcrystallization of silver chromate in the nervous tissue is much stronger than the common

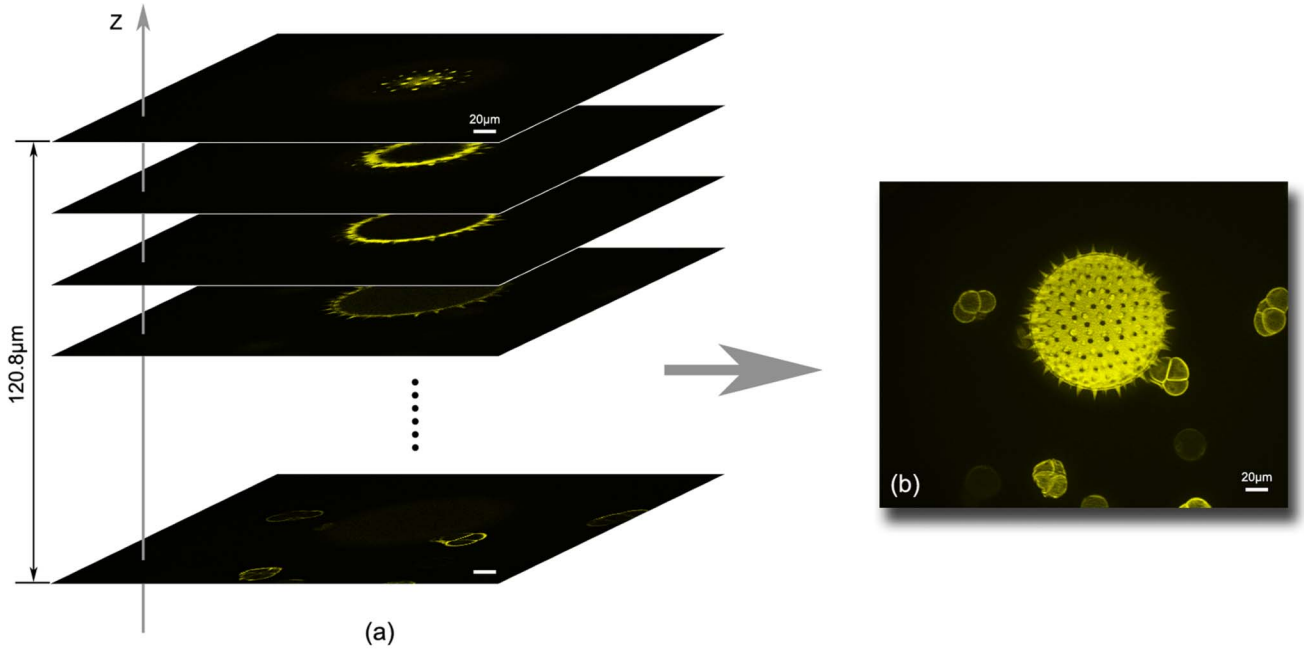

Figure 4 | Optical sectioning images of the thick volume structure of the mixed pollen grains. The signal came from the autofluorescence of sample with excitation using a 450 nm LED. (a) shows a stack of optically sectioned images comprised of 303 axial layers. (b) shows the maximum-intensity projection of the 303 planes along Z-axis over a 120.8 μm thickness (Supplementary Movie 1).

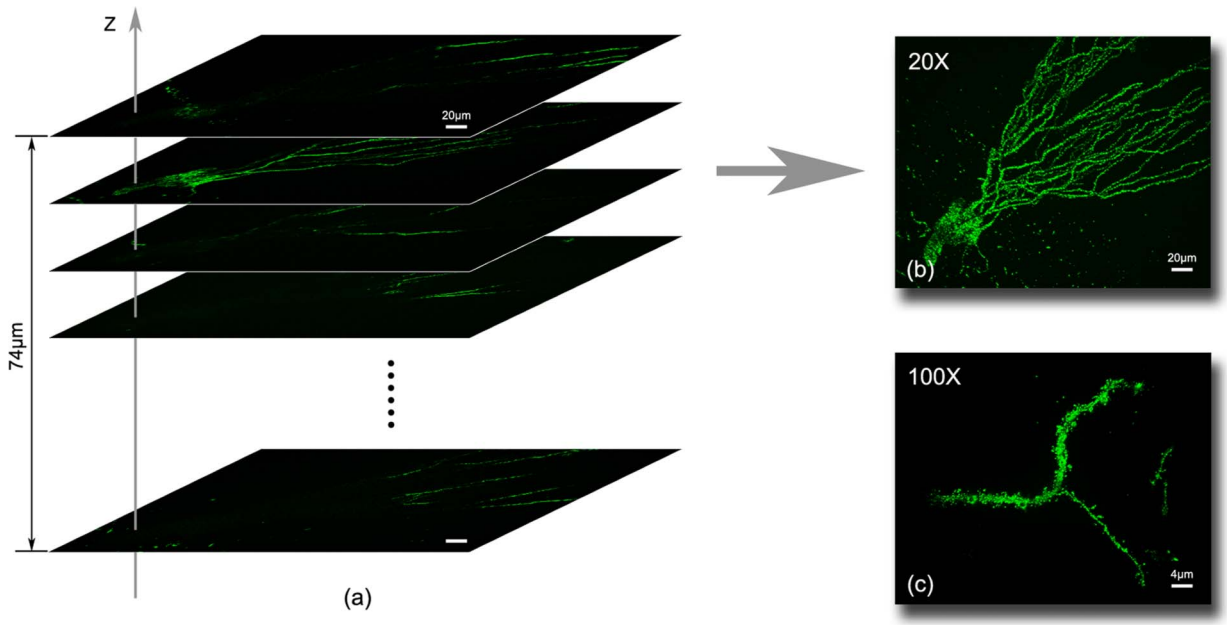

Figure 5 | Optically sectioned images of Golgi-stained mouse brain neuron cells. The signal was from the back-reflection and scattering of the microcrystaliliztion of silver chromate under the illumination of 450 nm LED light. (a) shows a stack of optically sectioned images comprised of 186 axial layers obtained with 20×, NA=0.6 objective. (b) shows the maximum-intensity projection of the 186 planes along Z-axis over a 74 μm thickness (Supplementary Movie 2). (c) shows the fine structure of the dendrite enlarged by using 100×, NA=1.49 objective (Supplementary Movie 3).

fluorescence, the exposure time of the CCD camera can be reduced, thus increasing the acquisition speed. The acquisition time of 186 slicing layers was 27 s, including 9 ms exposure time plus 36 ms readout time of the CCD camera for each raw image, 10 ms Z-stage settle time for each slicing layer, and 31 μs loading time for each DMD illumination fringe pattern. Figure 5(b) presents the maximum-intensity projection of the 186 planes along Z-axis. Figure 5(c) shows the fine structure of the dendrite enlarged by using 100×, NA=1.49 objective. The Supplementary Movie 2 and Supplementary Movie 3 show the "3D image" of the neuron cells with the 20× and 100× objectives, respectively. So far, we could realize maximal 200 μm penetration depth without obvious degradation of the image quality. In order to describe the sectioning strength of the SIM microscopy, a normalized spatial frequency $\nu=\lambda/(NA\cdot T)$ is introduced, where λ is the wavelength and T is the spatial periodicity of the projected fringe. The case of $\nu=0$ corresponds to the conventional wide-field microscope, while $\nu=1$ corresponds to the maximum sectioning strength[16]. In our experimental setup, the period of the illumination fringe was T=1225 nm at the 20×, NA=0.6 objective, which corresponds to $\nu=0.612$, from which the FWHM of 930 nm of sectioning strength was obtained.

Discussion

In most SIM systems, the generation of illumination fringe patterns is based on the laser beam interference. Commonly, microscope objectives with large numerical aperture are employed to get higher convergence angle, which determines the minimal fringe period illuminated on the sample. Taking an example for our case, where an oil immersion objective with NA=1.49 was used, the angular aperture is 78.6° (α=arcsin(1.49/1.52)=78.6°), which corresponds to a minimal fringe period of 230 nm at λ=450 nm if applying the two-beam interference geometry. This is the limitation of this approach. By contrast, in our low-coherence illumination fringe projection scheme, the minimum period of the fringe projected on the sample is limited by the Abbe resolution limit of the objective, which is about 151 nm. This means that our approach has the potential for higher spatial resolution compared with the interference approach.

As for the speed of data acquisition in the optical sectioning mode of the SIM system, it was mainly limited by the speed and sensitivity of the CCD camera, because both the switching time of DMD and the axial translation stage settle time are negligible. At the present version, we used a 1024×768 pixels commercial CCD camera with a maximum full-frame rate of 27 fps at its minimal exposure time. The maximum acquisition speed of 1.6×10^7 pixels/second was reached at the imaging of the Golgi-stained neuron cells. Higher acquisition speed could be achieved by using faster and sensitive cameras. For example, existing 4 M (2048×2048) pixels SCMOS cameras with a maximum full-frame rate of 100 fps will allow for about 3.14×10^8 pixels/second (7.5 s per volume for 186 slicing layers).

Although the lateral spatial resolution of 90 nm in XY-plane was achieved in the current system, the axial resolution is still ultimately limited by the point spread function (PSF) of the objective lens due to 2D fringe projection. Thus, the proposed approach does not lend itself to real 3D super-resolution, which is the disadvantage compared with the SIM microscopy using three beams interference illumination[9,14,28]. However, due to its simplicity, low-cost and fast imaging capability, the DMD-based LED-illumination SIM is still a useful tool in study of various biological samples. Particularly, it would be suitable for optical sectioning tomography application to improve resolution and image acquisition speed. Luo *et al.*[29] have developed a micro-optical sectioning tomography (MOST) system for obtaining the 3D structural data set of a Golgi-stained centimeter-sized whole mouse brain. The axial resolution depends on the positioning precision of the mechanical stage as well as the quality of the diamond knife. The acquisition speed relies on the precise slicing process, which is about 0.001 mm^3/s. Increasing the slicing thickness will improve the image acquisition speed, but also decrease the axial resolution. In view of the optical sectioning ability of 120 μm-penetration-depth and 930 nm-sectioning-strength obtained in our SIM system, we suggest to combine the two techniques in a hybrid arrangement. Firstly remove a thick slice (~120 μm) of the mouse brain with MOST, then perform the precisely optical sectioning inside the rest tissue with the SIM approach described in this paper. In this way, we would expect to achieve nearly isotropic sub-micron

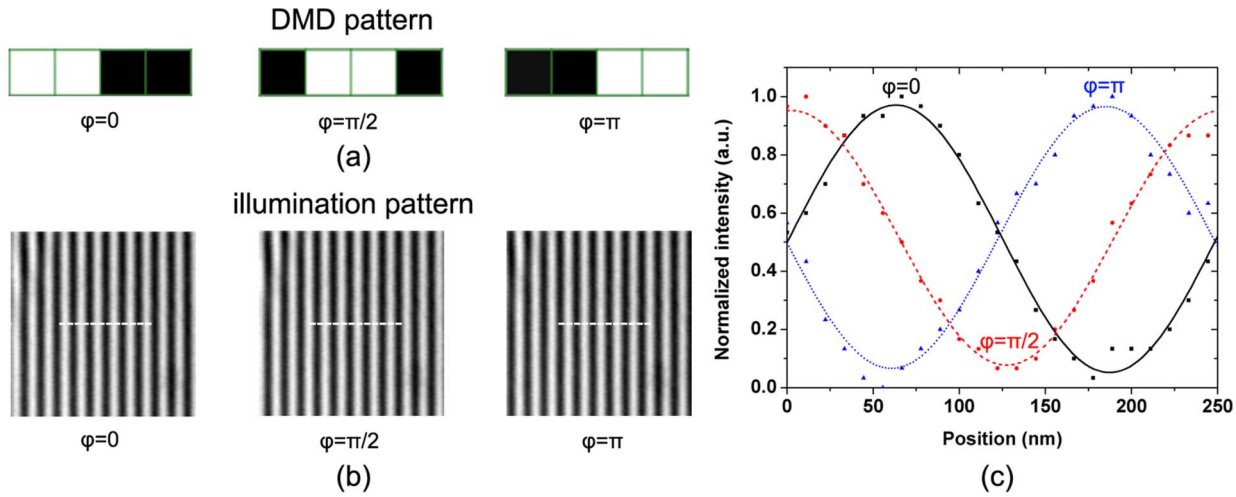

Figure 6 | Principle of generation of high-frequency phase-shifted sinusoidal fringe illumination with the DMD. (a) Binary patterns loaded on the DMD in one period of four pixels at three different phases; (b) corresponding illumination patterns captured in the focal plane of the objective lens (100×); (c) the measured intensity distribution curves of the illumination patterns along the cut-lines of (b) for the three phases of φ=0, π/2 and π, which show they are ideal sinusoidal fringes with a period of 245 nm and correct phase relations.

spatial resolution in all three dimensions, and dramatically increase the acquisition speed as well.

In conclusion, we have proposed a scheme of super-resolution and optical sectioning microscopy based on DMD fringe projection with low-coherence LED-illumination. We demonstrated that the setup has 90 nm lateral resolution, 120 μm penetration depth, and 930 nm sectioning strength with maximum acquisition speed of 1.6×10^7 pixels/second. The advantage of the proposed SIM setup includes its low-cost, ease of multi-wavelength switchable and speckle-noise-free. The 2D super-resolution and 3D optical sectioning modalities can be easily switched and applied to either fluorescent or non-fluorescent specimens.

Methods

Fringe projection by DMD. We used a DLP Discovery D4100 kit from Texas Instruments Inc. (Texas, USA) as an amplitude-only SLM for the fringe projection. This DMD chip can switch binary images of two grayscale levels 0 and 255 up to 32 KHz with a resolution of 1024×768 pixels with the pixel size of 10.8×10.8 μm^2. In common use of DMD fringe projection, the generation of a sinusoidal fringe of 256 grayscale levels requires at least 9 pixels for one period. This will apparently reduce the carrier frequency of the fringe and also limit the refreshing rate to 100 Hz. To solve this problem, a binary grating with a period of only 4 pixels is applied in our scheme, which enables fast transfer of patterns to the DMD up to 32 KHz refreshing rate. A sinusoidal intensity distribution projected in the focal plane of the objective is naturally obtained, because the objective lens automatically blocks the higher order spatial frequencies of the binary grating due to its limited bandwidth. Figure 6(a) shows the binary patterns loaded on the DMD chip in one period of 4 pixels at three phases. The corresponding illumination patterns captured in the focal plane of the objective are shown in Fig. 6(b). The period of the sinusoidal fringe is measured to be 245 nm in minimum (@100× objective) for the illumination patterns. From the intensity profile analysis of Fig. 6(c), it can be seen that the fringes are ideal sinusoidal and have the correct phase relations.

Imaging process and data analysis. The Fourier-based image reconstruction was processed according to the method of Gustafsson[17]. It should be noted that the initial phase is crucial for extraction of the high frequency components. It changes significantly with the sample location in the geometry of laser beams interference. Gustafsson[30] and Chang *et al.*[19] both used a complex linear regression algorithm to determine the initial phase for each orientation patterns, which is precise but rather time-consuming. In our geometry of fringe projection, the initial phase can be preset by the DMD for different orientations and remains unchanged for different sample location, which simplifies the image processing.

The full widths at half maximum (FWHM) of gold nano-particles were measured by fitting their intensity distributions to a Gaussian function with the ImageJ plugin (Point Spread Function Estimation Tool, Computational Biophysics Lab, ETH Zurich, Switzerland). For optical sectioning, the specimen was scanned axially by the motorized stage.

For each slice, three sub-images (denoted by I_{0°, I_{90° and I_{180°) with a phase-shift of $\delta=90^\circ$ between two adjacent images were acquired. After the recording process, each image triple was then processed according to Eq. (1) to obtain the sectioned images:

$$I_z(x,y)=\frac{1}{2}\sqrt{(2I_{90^0}-I_{0^0}-I_{180^0})^2+(I_{180^0}-I_{0^0})^2} \quad (1)$$

Materials. Gold nano-particles with a diameter of 80 nm (Nanocs Inc., New York, USA) were immersed in a PMMA film. The slice of mixed pollen grains was purchased from Carolina Biological Supply Inc. (Burlington, USA). Bovine Pulmonary Artery Endothelial (BPAE) cells slice stained with Mito Tracker Red CMXRos was purchased from Molecular Probes Inc. (Eugene, USA).

Golgi-Cox staining of mouse neuron cells. Male Sprague-Dawley rats weighting between 200 g and 230 g were provided by the Animal Center of the Fourth Military Medical University (FMMU), China. All experimental protocols were in accordance with the Guide line for the Animal Care and Use Committee for Research and Education of the FMMU. The rats were housed at 24±2°C with a 12 h light/12 h dark cycle, and food and water were available ad libitum. All efforts were made to minimize the number of animals used and their suffering. To prepare the material for modified rapid Golgi-Cox staining, Rats were first anesthetized with sodium pentobarbital (100 mg/kg body weight, i.p.) and perfused with 150 ml of 0.01 M phosphate-buffered saline (PBS; pH7.3), followed by 500 ml of 0.1 M phosphate buffer (PB; pH7.3) containing 0.5% (w/v) paraformaldehyde. The modified rapid Golgi-Cox staining was conducted according to a protocol reported previously[31] with slight modifications. In brief, the whole brain was dissected out and put into the Golgi-Cox solution (prepared at least 5 days before) at 37°C for 24 h in darkness. Then the brain was transferred into 30% sucrose solution until the brain sank. Sections of the thickness of 200 μm were cut with a vibratome (Microslicer DTM-1000; Dosaka EM, Kyoto, Japan), mounted on the gelatinized slides and air dried. Then, the sections were processed as follows: (1) Rinsed twice (5 min each) in distilled water to remove traces of impregnating solution; (2) Dehydrated in 50% alcohol for 5 min; (3) Kept in ammonia solution (3 : 1, ammonia: distilled water) for 5–10 min; (4) Rinsed twice (5 min each) in distilled water; (5) Kept in 5% sodium thiosulfate for 10 min in darkness; (6) Rinsed twice for 2 min each in distilled water; (7) Dehydrated twice (5–10 min each) in 70, 80, 95% and 100% ethanol and followed by transpiration with xylene. Finally the slides were mounted on a coverslip with Permount and lied out to dry for at least 7 days before observation.

1. Hell, S. W. Far-field optical nanoscopy. *Science* **25**, 1153–1158 (2007).
2. Hell, S. W. & Wichmann, J. Breaking the diffraction resolution limit by stimulated emission: stimulated-emission-depletion fluorescence microscopy. *Opt. Lett.* **19**, 780–782 (1994).
3. Vicidomini, G., Moneron, G., Han, K. Y., Westphal, V., Ta, V., Reuss, M., Engelhardt, J., Eggeling, C. & Hell, S. W. Sharper low-power STED nanoscopy by time gating. *Nat. Methods* **8**, 571–573 (2011).
4. Hanssen, E., Carlton, P., Deed, S., Klonis, N., Sedat, J., DeRisi, J. & Tilley, L. Whole cell imaging reveals novel modular features of the exomembrane system of the malaria parasite, Plasmodium falciparum. *Int .J. Parasitol.* **40**, 123–134 (2010).
5. Riglar, D. T., Richard, D., Wilson, D. W., Boyle, M. J., Dekiwadia, C., Turnbull, L., Angrisano, F., Marapana, D. S., Rogers, K. L., Whitchurch, C. B., Beeson, J. G., Cowman, A. F., Ralph, S. A. & Baum, J. Super-resolution dissection of coordinated

events during malaria parasite invasion of the human erythrocyte. *Cell Host Microbe.* **9**, 9–20 (2011).
6. Rust, M. J., Bates, M. & Zhuang, X. Sub-diffraction-limit imaging by stochastic optical reconstruction microscopy (STORM). *Nat. Methods* **3**, 793–796 (2006).
7. Huang, B., Wang, W., Bates, M. & Zhuang, X. Three-dimensional super-resolution imaging by stochastic optical reconstruction microscopy. *Science* **319**, 810–813 (2008).
8. Shroff, H., Galbraith, C. G., Galbraith, J. A. & Betzig, E. Live-cell photoactivated localization microscopy of nanoscale adhesion dynamics. *Nat. Methods* **5**, 417–423 (2008).
9. Schermelleh, L., Carlton, P. M., Haase, S., Shao, L., Winoto, L., Kner, P., Burke, B., Cardoso, M. C., Agard, D. A., Gustafsson, M. G. L., Leonhardt, H. & Sedat, J. W. Subdiffraction multicolor imaging of the nuclear periphery with 3D structured illumination microscopy. *Science* **320**, 1332–1336 (2008).
10. Fitzgibbon, J., Bell, K., King, E. & Oparka, K. Super-resolution imaging of plasmodesmata using three-dimensional structured illumination microscopy. *Plant Physiol.* **153**, 1453–1463 (2010).
11. Markaki, Y., Smeets, D., Fiedler, S., Schmid, V. J., Schermelleh, L., Cremer, T. & Cremer, M. The potential of 3D-FISH and super-resolution structured illumination microscopy for studies of 3D nuclear architecture. *Bio. Essays* **34**, 412–426 (2012).
12. Keller, P. J., Schmidt, A. D., Santella, A., Khairy, K., Bao, Z., Wittbrodt, J. & Stelzer, E. H. K. Fast, high-contrast imaging of animal development with scanned light sheet-based structured-illumination microscopy. *Nat. Methods* **7**, 637–642 (2010).
13. Hirvonen, L. M., Wicker, K., Mandula, O. & Heintzmann, R. Structured illumination microscopy of a living cell. *Eur. Biophys. J.* **38**, 807–812 (2009).
14. Shao, L., Kner, P., Rego, E. H. & Gustafsson, M. G. L. Super-resolution 3D microscopy of live whole cells using structured illumination. *Nat. Methods* **8**, 1044–1046 (2011).
15. Kner, P., Chhun, B. B., Griffis, E. R., Winoto, L. & Gustafsson, M. G. L. Super-resolution video microscopy of live cells by structured illumination. *Nat. Methods* **6**, 339–342 (2009).
16. Neil, M. A. A., Juskaitis, R. & Wilson, T. Method of obtaining optical sectioning by using structured light in a conventional microscope. *Opt. Lett.* **22**, 1905–1907 (1997).
17. Gustafsson, M. G. L. Surpassing the lateral resolution limit by a factor of two using structured illumination microscopy. *J. Microsc.* **198**, 82–87 (2000).
18. Gustafsson, M. G. L. Nonlinear structured-illumination microscopy: Wide-field fluorescence imaging with theoretically unlimited resolution. *PNAS* **102**, 13081–13086 (2005).
19. Chang, B. J., Chou, L. J., Chang, Y. C. & Chiang, S. Y. Isotropic image in structured illumination microscopy patterned with a spatial light modulator. *Opt. Express* **17**, 14710–14721 (2009).
20. Fiolka, R., Beck, M. & Stemmer, A. Structured illumination in total internal reflection fluorescence microscopy using a spatial light modulator. *Opt. Lett.* **33**, 1629–1631 (2008).
21. Liang, M., Stehr, R. L. & Krause, A. W. Confocal pattern period in multiple-aperture confocal imaging systems with coherent illumination. *Opt. Lett.* **22**, 751–753 (1997).
22. Zheng, J. Y., Pasternack, R. M. & Boustany, N. N. Optical scatter imaging with a digital micromirror device. *Opt. Express* **17**, 20401–20414 (2009).
23. Jiang, S. H. & Walker, J. G. Speckle-illuminated fluorescence confocal microscopy, using a digital micro-mirror device. *Meas. Sci. Technol.* **20**, 065501 (2009).
24. Zhang, S., Van Der Weide, D. & Oliver, J. Superfast phase-shifting method for 3-D shape measurement. *Opt. Express* **18**, 9684–9689 (2010).
25. Fukano, T. & Miyawaki, A. Whole-field fluorescence microscope with digital micromirror device: imaging of biological samples. *Appl. Opt.* **42**, 4119–4124 (2003).
26. Fukano, T., Sawano, A., Ohba, Y., Matsuda, M. & Miyawaki, A. Differential Ras activation between caveolae/raft and non-raft microdomains. *Cell Struct. Funct.* **32**, 9–15 (2007).
27. McMackin, L. & Chatterjee, S. TIR prism to separate incident light and modulated light in compressive imaging device. *U.S. Patent* 20120038819A1 (Feb. 16, 2012).
28. Gustafsson, M. G. L., Shao, L., Carlton, P. M., Wang, C. J. R., Golubovskaya, I. N., Cande, W. Z., Agard, D. A. & Sedat, J. W. Three-dimensional resolution doubling in wide-field fluorescence microscopy by structured illumination. *Biophys. J.* **94**, 4957–4970 (2008).
29. Li, A., Gong, H., Zhang, B., Wang, Q., Yan, C., Wu, J., Liu, Q., Zeng, S. & Luo, Q. Micro-optical sectioning tomography to obtain a high-resolution atlas of the mouse brain. *Science* **330**, 1404–1408 (2010).
30. Gustafsson, M. G. L. Doubling the lateral resolution of wide-field fluorescence microscopy using structured illumination. *Proc. SPIE* **3919**, 141–150 (2000).
31. Ranjan, A. & Mallick, B. N. A modified method for consistent and reliable Golgi-cox staining in significantly reduced time. *Front Neurol.* **1**, 157 (2010).

Acknowledgments

This research is supported by the National Basic Research Program (973 Program) of China under Grant No. 2012CB921900, and the Natural Science Foundation of China (NSFC) under Grant Nos. 61077005, 61275193.

Author contributions

Ming Lei built up the optical hardware and Dan Dan wrote the software for controlling the system and image acquisition. Baoli Yao designed the experiments, developed the concept and supervised the whole project. Andreas Zumbusch contributed to the design of the system and considerably improved the manuscript presentation. Wen Wang and Liang Xia prepared for the samples. Martin Winterhalder, Yujiao Qi and Shaohui Yan processed and visualized the data. Yanlong Yang, Peng Gao, Tong Ye and Wei Zhao provided technical support. All authors contributed to the scientific discussion and revision of the article.

Additional information

Supplementary information accompanies this paper at http://www.nature.com/scientificreports

Competing financial interests: The authors declare no competing financial interests.

How to cite this article: Dan, D. *et al.* DMD-based LED-illumination Super-resolution and optical sectioning microscopy. *Sci. Rep.* **3**, 1116; DOI:10.1038/srep01116 (2013).